



**Nanobodies Against the Metal Binding Domains of ATP7B as  
Tools to Study Copper Transport in the Cell**

Journal:	<i>Metallomics</i>
Manuscript ID	MT-ART-08-2020-000191.R1
Article Type:	Paper
Date Submitted by the Author:	08-Oct-2020
Complete List of Authors:	<p>Uhlemann, Eva-Maria; University of Saskatchewan, Biochemistry, Microbiology and Immunology</p> <p>Yu, Corey; University of Saskatchewan, Biochemistry, Microbiology and Immunology</p> <p>Patry, Jaala; University of Saskatchewan, Biochemistry, Microbiology and Immunology</p> <p>Dolgova, Natalia; University of Saskatchewan, Biochemistry, Microbiology and Immunology</p> <p>Lutsenko, Svetlana; Johns Hopkins University, Physiology</p> <p>Muyldermans, Serge; Vrije Universiteit Brussel, Cellular and Molecular Immunology</p> <p>Dmitriev, Oleg Y.; University of Saskatchewan, Biochemistry, Microbiology and Immunology</p>

1  
2 Human copper transporter ATP7B (Wilson disease protein) is a multidomain membrane protein  
3 with poorly understood mechanism and complex regulation of enzymatic activity and intracellular  
4 localization. ATP7B is a challenging target both for structural biology and for in-cell studies. We have  
5 developed and characterized a large panel of Nanobodies targeting various metal binding domains of  
6 ATP7B, with wide range of affinity, different copper dependence profile, and diverse modulatory  
7 effects on ATP7B activity and protein dynamics. These novel tools are urgently needed to solve the  
8 high-resolution structure and to understand the mechanism of copper transport, regulation and  
9 intracellular trafficking of ATP7B.  
10  
11  
12  
13  
14  
15  
16  
17  
18  
19  
20  
21  
22  
23  
24  
25  
26  
27  
28  
29  
30  
31  
32  
33  
34  
35  
36  
37  
38  
39  
40  
41  
42  
43  
44  
45  
46  
47  
48  
49  
50  
51  
52  
53  
54  
55  
56  
57  
58  
59  
60

## Nanobodies Against the Metal Binding Domains of ATP7B as Tools to Study Copper Transport in the Cell

Eva-Maria E. Uhlemann<sup>a</sup>, Corey H. Yu<sup>a</sup>, Jaala Patry<sup>a</sup>, Natalia Dolgova<sup>a</sup>, Svetlana Lutsenko<sup>b</sup>, Serge Muyldermans<sup>c</sup>, and Oleg Y. Dmitriev<sup>a\*</sup>

### Abstract

Nanobodies are genetically engineered single domain antibodies derived from the unusual heavy-chain only antibodies found in llamas and camels. Small size of the Nanobodies and flexible selection schemes make them uniquely versatile tools for protein biochemistry and cell biology. We have developed a panel of Nanobodies against the metal binding domains of the human copper transporter ATP7B, a multidomain membrane protein with a complex regulation of enzymatic activity and intracellular localization. To enable the use of the Nanobodies as tools to investigate copper transport in the cell, we characterized their binding sites and affinity by isothermal titration calorimetry and NMR. We have identified Nanobodies against each of the first four metal binding domains of ATP7B, with a wide affinity range, as evidenced by dissociation constants from below  $10^{-9}$  to  $10^{-6}$  M. We found both the inhibitory and activating Nanobodies among those tested. The diverse properties of the Nanobodies make the panel useful for the structural studies of ATP7B, immunoaffinity purification of the protein, modulation of its activity in the cell, protein dynamics studies, and as mimics of copper chaperone ATOX1, the natural interaction partner of ATP7B.

---

<sup>a</sup>Department of Biochemistry, Microbiology and Immunology, University of Saskatchewan, Saskatoon, SK, Canada

<sup>b</sup>Department of Physiology, Johns Hopkins University School of Medicine, Baltimore, MD, USA

<sup>c</sup>Cellular and Molecular Immunology, Vrije Universiteit Brussel, Belgium

\*Corresponding Author: Oleg Dmitriev; e-mail: [oleg.dmitriev@usask.ca](mailto:oleg.dmitriev@usask.ca)

## Introduction

Nanobodies are single-domain immunoaffinity reagents derived from the unusual type of antibodies that consist of heavy chains only and are produced in llamas and camels, along with the conventional IgG antibodies<sup>1</sup>. To make Nanobodies, the animal is immunized with the antigen of interest. When the immune response develops, a cDNA library encoding the variable heavy chain domains (VHH) is generated from the mRNA pool of the peripheral blood mononuclear cells. Following selection for binding affinity and specificity, the chosen VHH clones are expressed in *E. coli* and then purified by ion-metal affinity chromatography and gel filtration. A detailed protocol for Nanobody production has been published<sup>2</sup>.

Nanobodies have been used extensively in structural biology to assist crystallization of difficult proteins<sup>3-7</sup>, stabilize desired protein conformations<sup>8-11</sup>, and study protein dynamics by NMR<sup>12-14</sup>. Due to their small size, amenability to chemical and genetic derivatization, as well as ease of production of the recombinant protein in *E. coli*, Nanobodies are often more versatile tools of molecular biology than the conventional antibodies, or their fragments. In cell biology, Nanobodies have been used for protein tracking<sup>15,16</sup>, manipulation of intracellular localization of proteins and protein complexes<sup>17-19</sup>, and targeted protein degradation<sup>20-22</sup>. For manipulating proteins in living cells, Nanobodies can be expressed inside the cell, or modified to make them cell permeable<sup>23,24</sup>. Because of their advantageous properties, including better tissue penetrating ability, compared to the conventional antibodies, Nanobodies attract growing interest for imaging and immunotherapy in cancer and other conditions<sup>25,26</sup>, including neurodegenerative disorders<sup>27</sup> and, very recently, coronavirus infections<sup>28</sup>. The first Nanobody drug, Caplacizumab, has been recently approved for treatment of acquired thrombotic thrombocytopenic purpura<sup>29</sup>.

We have developed a panel of Nanobodies to investigate the mechanism of regulation of the human copper transporter ATP7B, a multidomain membrane protein with complex domain dynamics and copper-dependent intracellular trafficking. ATP7B is located in the *trans*-Golgi network (TGN), where it transports copper to the maturing metalloproteins. When copper level in the cell increases, ATP7B moves to the cytosolic vesicles, where it accumulates excess copper in the vesicular lumen for subsequent excretion from the cell by exocytosis, and to the plasma membrane, where it may directly transport copper out of the cell<sup>30</sup>. The loss of ATP7B activity due to mutations causes Wilson disease, a chronic disorder of copper metabolism, which damages the liver and causes a variety of neurological and psychiatric symptoms<sup>31,32</sup>.

ATP7B is a multidomain protein with an overall architecture characteristic of the P-type ATPases, such as Ca<sup>2+</sup>-ATPase (SERCA)<sup>33</sup> or Na<sup>+</sup>,K<sup>+</sup>-ATPase<sup>34</sup>. A unique feature of ATP7B and closely related copper transporter ATP7A is a chain of six metal-binding domains (MBD), connected by flexible linkers of various length (Fig. 1, A).

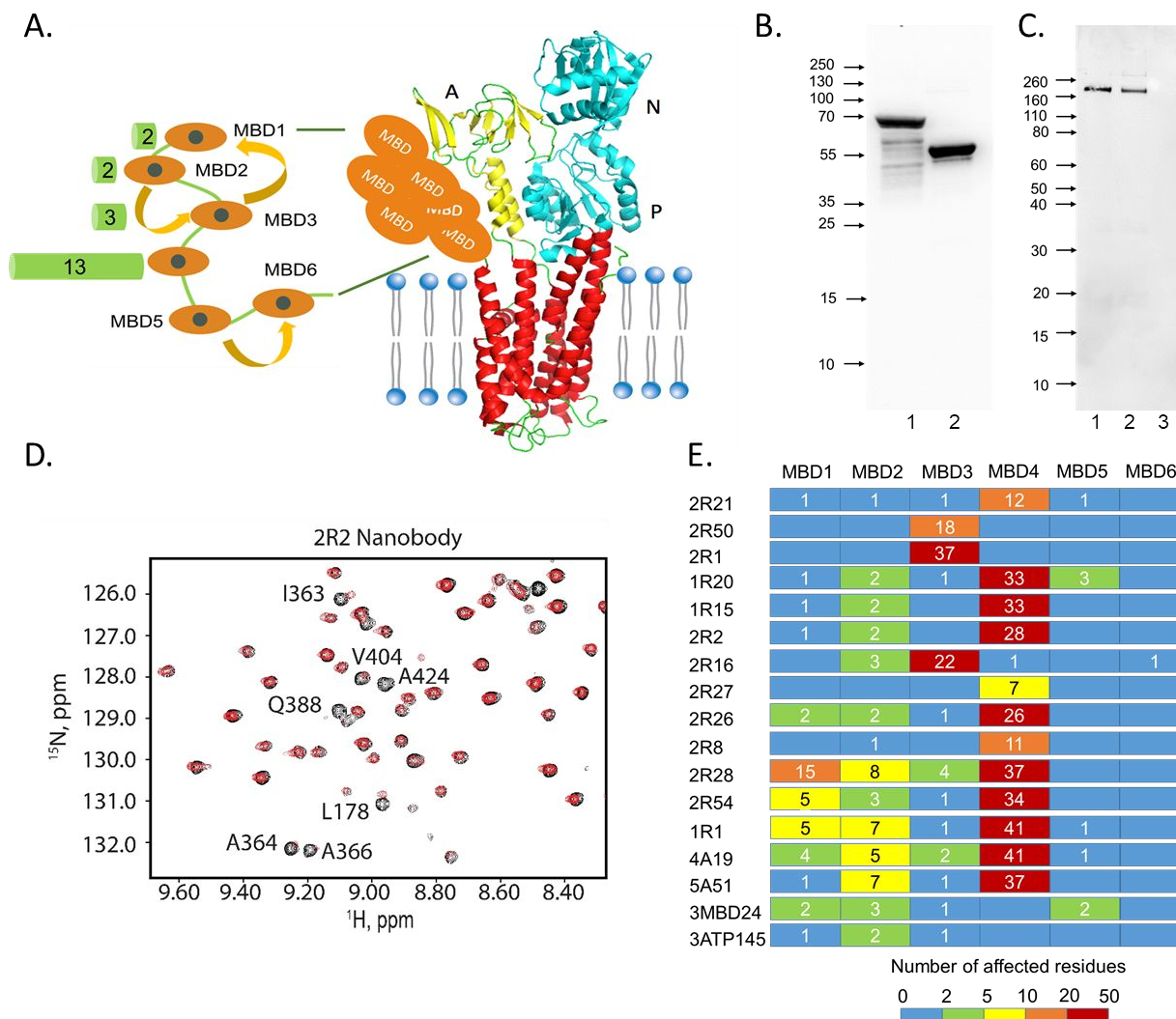


**Fig.1 Domain structure of ATP7B and overview of the Nanobodies against ATP7B metal-binding domains** (A) ATP7B is composed of six metal binding domains (MBD, orange), eight transmembrane helices (red), actuator domain (A-domain, yellow), and ATP-binding domain, consisting of N- and P- subdomains (cyan). Arrows indicate domain-domain interactions, and the green bars show the number of Nanobodies targeting each domain. (B, C) Western blots of purified MBD1-6 (B, lane 1), MBD1-4 (B, lane 2), and HEK293 expressing recombinant wild type ATP7B (C, lane 1), D1027A-ATP7B (C, lane 2) or endogenous ATP7B only (C, lane 3) with 2R21 Nanobody against MBD4. (D) Overlay of an uncrowded region of the 900 MHz TROSY spectra of MBD1-6 with (red) and without (black) the 2R2 Nanobody. Sequential amino acid residue assignments of the signals affected by the Nanobody binding are shown. The 2R2 Nanobody binds in the intermediate exchange regime manifested both by peak shifts and intensity loss. (E) Mapping Nanobody binding site by NMR. Number of amino acid residue signals in the MBD1-6 NMR spectra affected by the addition of the selected Nanobodies in each of the MBDS.

Each domain has a ferredoxin fold and binds one Cu(I) atom at the conserved CxxC motif. In the cell, MBDS receive copper from a cytosolic chaperone protein ATOX1, which is structurally

1  
2  
3 rather similar to the MBDs<sup>35</sup>. There is no high-resolution structure of the complete ATP7B, and  
4 the sequence of copper transfer steps within the protein is not known. Copper binding to one or  
5 several MBDs appears not only to be the first step in copper translocation across the membrane,  
6 but also regulate enzymatic activity and trafficking of ATP7B through the changes in the dynamics  
7 and interactions of these domains.  
8  
9

10  
11 NMR studies of the MBD1-6 chain<sup>36,37</sup> show that the individual domains do not fold together  
12 into a compact structure, but experience largely independent motions, with the exception of MBDs  
13 5-6, which form a stable unit<sup>38</sup>. At the same time, biochemical evidence indicates Cu-dependent  
14 interactions and cross-talk between individual MBDs<sup>39-42</sup>. Using Nanobodies as probes of  
15 molecular dynamics we have shown by NMR that MBD1-3 associate in a dynamically correlated  
16 domain group maintained by weak interactions, whereas MBD4 shows largely independent  
17 dynamics<sup>14,43</sup>. Copper transfer from ATOX1 disrupts MBD1-3 interactions increasing domain  
18 mobility and activating ATP-dependent copper transport<sup>43</sup>. Remarkably, the 2R50 Nanobody  
19 targeting MBD3 has a similar effect on domain dynamics, also causing dissociation of the MBD1-3  
20 domain group, which suggests using the Nanobodies as mimics of ATOX1 in dissecting complex  
21 relationship between the regulatory and the catalytic copper transfer between ATOX1 and ATP7B,  
22 and between the multiple copper-binding sites in ATP7B. Nanobodies 2R21 and 4A19 have been  
23 used previously to modulate intracellular localization of ATP7B<sup>14</sup>.  
24  
25  
26  
27  
28  
29

30 To realize the full potential of Nanobodies for studying the mechanism of copper transport in the  
31 cell, we have characterized the binding properties of a diverse panel of Nanobodies against metal-  
32 binding domains of ATP7B, in comparison to the copper chaperone ATOX1.  
33  
34

## 35 **Experimental**

### 36 *Generation of Nanobodies against the metal-binding domains*

37  
38 Alpaca was immunized with the purified N-terminal fragment of ATP7B containing all six  
39 metal-binding domains (MBD1-6) fused to maltose-binding protein (MBP), in either metal-free or  
40 copper-bound form and the Nanobodies were generated as described previously<sup>14</sup>. Among the  
41 Nanobodies characterized in detail here (Table 1), 2R50, 2R21, and 1R1 were raised against Cu-  
42 MBD1-6, and 4A19 against *apo*-MBD1-6. Briefly, two variable heavy chain (VHH) libraries  
43 containing about  $4 \times 10^8$  (Cu-MBD1-6) and  $8 \times 10^8$  (*apo*-MBD1-6) independent transformants  
44 were constructed and screened for the presence of antigen-specific Nanobodies using phage  
45 display. Each library was subjected to two consecutive rounds of panning, performed on a solid-  
46 phase plate coated with MBD1-6-MBP fusion, in the metal-free or copper-loaded form, as  
47 appropriate, using soluble MBP for negative selection. The clones producing MBD1-6 specific  
48 Nanobodies were then selected by ELISA. Nanobodies against MBD1 and MBD2 were  
49 subsequently selected from the combined original libraries in a similar fashion, using respective  
50 MBDs in the copper-free form (*apo*-form) as target antigens, and *apo*-MBD4 for negative  
51  
52  
53  
54  
55  
56  
57  
58  
59  
60

1  
2  
3 selection. Selected Nanobodies were expressed in *E. coli* as fusions with the N-terminal pelB  
4 sequence for periplasm targeting, and C-terminal hexahistidine tag for purification by immobilized  
5 metal affinity chromatography. Nanobodies were purified by the affinity chromatography on Ni-  
6 NTA resin.  
7  
8  
9

#### 10 *Purification of metal-binding domain constructs and ATOX1*

11 Individual MBDs 1, 2 and 4, MBD1-4 fragment (ATP7B residues 1-430), MBD1-6 fragment  
12 (residues 1-633), and ATOX1 were expressed in *E. coli* as fusions with the chitin-binding domain  
13 and intein, and purified by affinity chromatography on chitin resin combined with intein cleavage  
14 by dithiothreitol essentially as described previously <sup>14</sup>.  
15  
16  
17

#### 18 *Isothermal titration calorimetry*

19 For ITC experiments, the Nanobodies, MBD1-4 and ATOX1 were dialyzed against degassed  
20 50 mM HEPES, pH 7.4, 150 mM NaCl, 5 mM TCEP under argon. Where appropriate, MBD1-4  
21 or ATOX1 were loaded with copper by adding freshly prepared 9 mM CuCl solution in 1 M NaCl  
22 containing 0.01 M HCl, in the equimolar ratio of copper to the copper-binding sites prior to dialysis.  
23 ITC was performed on a TA Instruments (New Castle, DE) Low Volume Nano calorimeter using  
24 ITCRun software and analyzed with NanoAnalyze software (TA Instruments) using a single  
25 binding site independent model setting. A 0.13-0.6 mM solution of a Nanobody was titrated into  
26 0.17 ml of 0.01-0.05 mM target protein, 1.5-2.5  $\mu$ l per injection at 300 s intervals at 30°C under  
27 constant stirring at 300 r.p.m. Dilution heat correction was applied by titrating the Nanobody into  
28 the ITC buffer containing no protein. Most of the titrations were performed in duplicate or triplicate.  
29  
30  
31  
32  
33

#### 34 *ATPase activity measurements*

35 The wild type and catalytically inactive D1027A variant of ATP7B were expressed in HEK293  
36 cells, and the cell membrane fraction was prepared as described previously <sup>44</sup>. ATPase activity of  
37 the membranes was determined from the linear time course of inorganic phosphate liberation in a  
38 buffer containing 50 mM MES, pH 6.0, 10% glycerol, 150 mM NaCl, 3 mM MgCl<sub>2</sub>, 0.5 mM ATP  
39 and 5  $\mu$ g membrane protein in a volume of 40  $\mu$ l at 37°C. Phosphate concentration was measured  
40 by malachite green assay <sup>45,46</sup> in a microplate format. ATP7B activity was calculated as a  
41 difference between the total ATPase activity of the wild type ATP7B and D1027A-ATP7B  
42 membranes. Thus ATPase activity unrelated to ATP7B, as well as activity of the endogenous  
43 ATP7B present in HEK293 membranes at low level was subtracted from the total ATPase activity.  
44 Copper stimulation of ATP7B activity was measured in the presence of 10  $\mu$ M ATOX1-Cu.  
45  
46  
47  
48  
49

#### 50 *Small angle X-ray scattering*

51 Purified MBD1-4 was dialyzed against 50 mM HEPES, pH 7.4, 150 mM NaCl, and 0.6 mM  
52 TCEP. SAXS data collection, buffer subtraction and data averaging was performed at SIBYLS  
53 beamline, Lawrence Berkley Laboratory <sup>47</sup>, using in-line size exclusion chromatography (SEC) on  
54 Agilent 1260 HPLC system with a Shodex Protein KW-802.5 column eluted with dialysis buffer  
55  
56  
57  
58  
59  
60

1  
2  
3 at a flow rate of 0.5 ml/min. DAMMIF<sup>48</sup> was used to create 10 *ab initio* dummy atom models,  
4 which were then averaged with DAMAVER<sup>49</sup>. HADDOCK<sup>50</sup> was used for modeling the MBD1-  
5 MBD3 interaction by incorporating <sup>1</sup>H, <sup>15</sup>N HSQC chemical shift perturbation data (6). The top-  
6 scoring model of MBD1-MBD3 and high resolution solution structures of MBD2 and MBD4 were  
7 fitted into the apo-MBD1-4 SAXS envelope using BUNCH<sup>51</sup>.  
8  
9

### 10 11 *NMR spectroscopy*

12 NMR samples contained 100-120 μM <sup>15</sup>N-labelled MBD1-6, 50 mM HEPES-Na, pH 7.4, 50  
13 mM NaCl, 5 mM TCEP, 5% (v/v) D<sub>2</sub>O and 0.5 mM 2,2-dimethyl-2-sila-pentane-5-sulfonate  
14 (DSS) for the chemical shift referencing. The <sup>1</sup>H,<sup>15</sup>N-TROSY<sup>52</sup> experiments were recorded at  
15 310K on a 900 MHz NMR spectrometer equipped with a triple-resonance cold probe with z-axis  
16 gradients. The previously published backbone chemical shift assignments<sup>36</sup> were used for  
17 mapping the Nanobody binding sites. Combined chemical shift change was calculated as  $[(\Delta\delta_{\text{NH}}^2 +$   
18  $\Delta\delta_{\text{N}}^2/25)/2]^{1/2}$ , where  $\Delta\delta_{\text{NH}}$  and  $\Delta\delta_{\text{N}}$  are the chemical shifts changes of the amide proton and  
19 nitrogen respectively. Nanobodies were added to the protein at 1:1 molar ratio.  
20  
21  
22  
23

### 24 *Western blot analysis*

25 Proteins were resolved by SDS-PAGE on 10% Schagger –von Jagow<sup>53</sup> or Laemmli<sup>54</sup> gels and  
26 transferred to the nitrocellulose membrane using semi-dry method. The blots were blocked with  
27 QIAGEN blocking reagent in TBS, and washed with TBS. The blots were then incubated with an  
28 appropriate Nanobody at 0.6 μg/ml or 6 μg/ml, as indicated, in TBS containing QIAGEN blocking  
29 agent, as primary antibody. Following three washes in TBS, the blots were incubated for 4 hours  
30 at room temperature with anti-hexahistidine horseradish peroxidase conjugated antibodies  
31 (“Qiagen”) at 1:2,500 dilution in TBS. Following washes with TBS, the antibody binding was  
32 visualized by enhanced chemiluminescence (ECL) detection using Syngene imager.  
33  
34  
35  
36  
37  
38

## 39 **Results and Discussion**

40  
41 We created a library of the antibody variable heavy chain domain (VHH) cDNA, which contains  
42 a total of  $1.2 \times 10^9$  independent clones, following immunization of alpaca with a fragment  
43 containing all six metal-binding domains (MBD1-6) as an antigen. After the first round of  
44 selection, we chose sixteen Nanobodies for further characterization. The Nanobodies reacted with  
45 purified MBD1-4 and MBD1-6 on a Western blot (Fig. 1, B, and Fig. S1), and some also detected  
46 full-length ATP7B in the membrane preparations from HEK293 cells (Fig. 1, C, Fig. S1).  
47  
48  
49

50  
51 The binding sites for these Nanobodies were mapped by NMR chemical shift perturbation  
52 analysis with <sup>15</sup>N-labeled MBD1-6<sup>14</sup>, (Fig 1D, E, Supplementary Data). The domain that contains  
53 the primary Nanobody binding site would show multiple changes in the chemical shifts or intensity  
54 of the backbone amide signals, depending on the NMR exchange regime, a property of the protein  
55  
56  
57  
58  
59  
60

complex related to the binding affinity of the Nanobody. In some cases, the pattern of the chemical shift changes allows even more precise epitope mapping and modeling the MBD-Nanobody complex, as shown for the 2R50 Nanobody binding to MBD3 (Fig. 2 A). Some of the Nanobodies, e.g. 2R21, 2R50, 2R1, clearly bind to a single domain, while others, e.g. 2R28 and 2R1 appear to show some cross-reactivity with two or three domains.

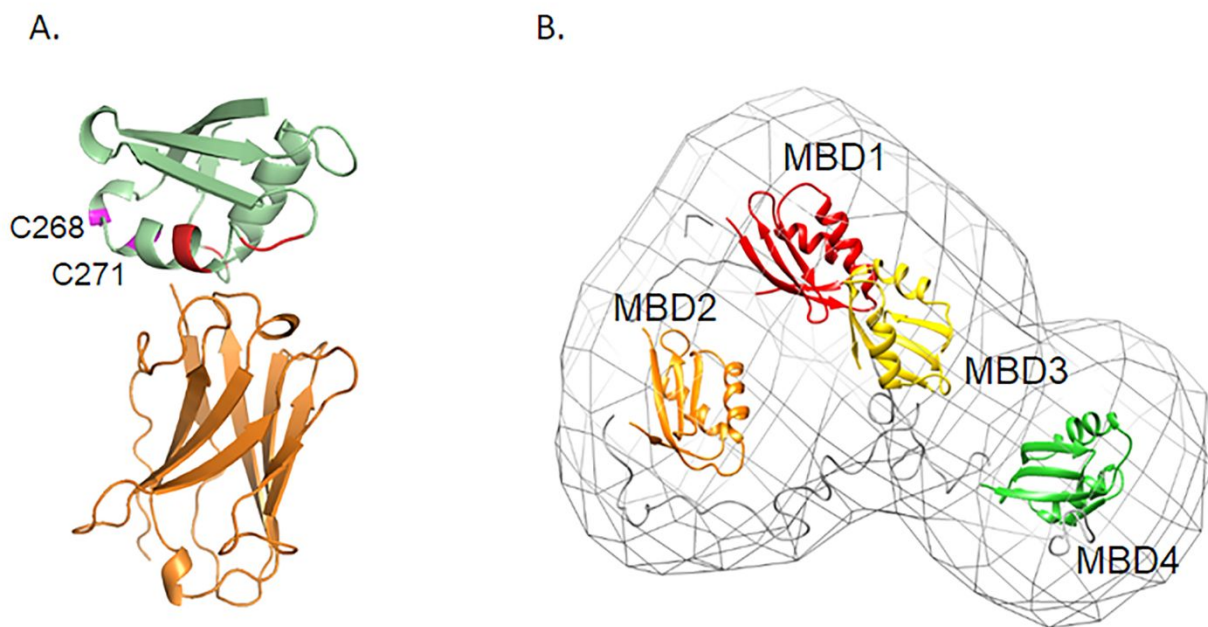


**Fig. 2 Interaction of the metal binding domains with Nanobodies (A)** The 2R50 Nanobody bound to MBD3. The model was calculated by HADDOCK using chemical shift perturbation data<sup>14</sup>. MBD3 is *green* and the Nanobody is *orange*. Amino acid residues in MBD3 showing the largest chemical shift changes upon 2R50 binding ( $\Delta\delta > 0.4$  p.p.m.) are in *red*. The copper-binding cysteines are in *magenta*. **(B)** Space envelope of *apo*-MBD1-4 determined by SAXS with the individual domain positions shown.

In the initial panel, we expected to find Nanobodies against all or most of the six metal-binding domains of ATP7B. However, out of sixteen Nanobodies, thirteen were found to bind to MBD4 and three to MBD3 (Fig. 1, A). There were no binders to either MBD1-2 or MBD5-6. This disproportionate representation of Nanobodies against MBD4 is likely explained by the greater surface exposure of this domain, compared to the others. MBD1-6 appears to consist of two separate domain groups, MBD1-3<sup>14</sup> and MBD5-6<sup>38</sup>, with MBD4 showing no association with other domains and largely independent dynamics. While Nanobodies against MBD1-6 proved to be very useful tools for investigating MBD1-6 conformation and dynamics<sup>14</sup>, we were also interested in the Nanobodies against MBD1 and MBD2, because copper-dependent changes in dynamics and conformation of MBD1-3 domain group appear to be the first step in regulating activity and, possibly, the intracellular localization of ATP7B. To select Nanobodies against

MBD1 and MBD2, we rescreened the original VHH library, this time using purified individual MBD1 and MBD2 as immobilized antigens for positive selection, and soluble MBD4 for negative selection, to eliminate variants with cross-reactivity between these domains. This selection round produced four Nanobodies with distinct amino acid sequences, two binding to MBD1 (3ATP7 and 3ATP145) and two to MBD2 (3MBD10 and 3MBD24), as determined by ELISA (Fig. S2) Because Nanobodies against MBD4 were strongly overrepresented in our initial panel, and many of them appeared to have rather similar binding properties, as indicated by NMR spectroscopy, we limited the number of Nanobodies chosen for further analysis. The Nanobodies for detailed characterization were selected to target each of the first four domains, represent a wide range of affinities, based on the NMR data, and include both those raised against *apo*- and Cu-bound forms of MBD1-6.

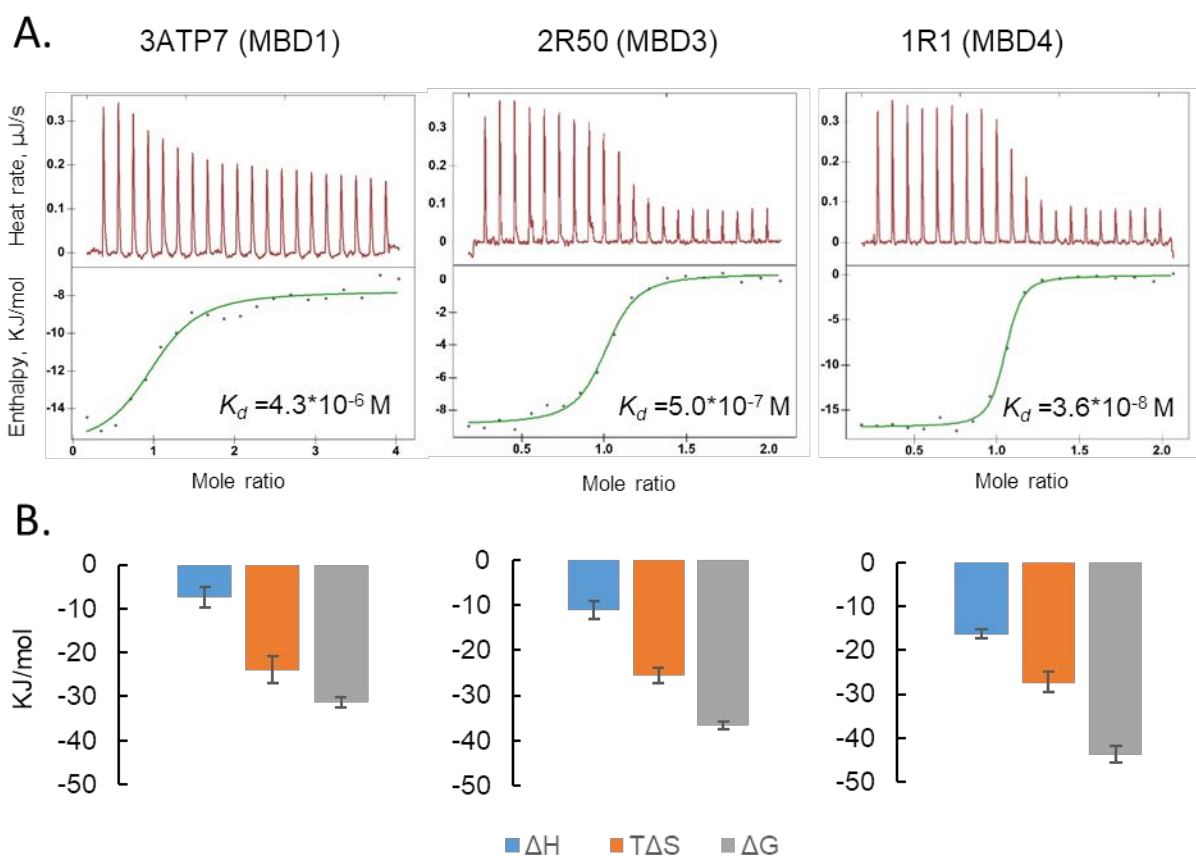


**Fig. 3 Thermodynamic parameters of Nanobody binding to MBD1-4. (A)** Thermograms and dissociation constants of Nanobodies representing various binding affinity ranges. **(B)** Enthalpic and entropic contributions to the free energy change Nanobody binding.

Initial NMR analysis suggested that Nanobodies in our panel may have rather different binding affinities. This is notable, because different applications require different Nanobody affinity.

Protein dynamics studies by NMR may favor lower binding affinity. On the other hand, using Nanobodies for immunoaffinity purification (Fig. S3), or as crystallization chaperones, requires tight binding, while in-cell applications may benefit from either tight or moderate binding, depending on the purpose of the experiment. With this in mind, we set out to determine binding affinity of the selected Nanobodies by isothermal titration calorimetry (ITC, Fig. 3).

We investigated Nanobody binding to the MBD1-4 fragment of ATP7B (residues 1-430, Fig. 2 B). Because MBDs interact with each other, and because the interdomain loop regions may contribute to the epitope formation, this is a more physiologically relevant model, than the isolated individual domains. We selected from one to three Nanobodies for each target domain, from MBD1 to MBD4, and measured binding to the copper-free MBD1-4 fragment. Binding affinity, as measured by the dissociation constant ( $K_d$ ) ranged from approximately  $4 \times 10^{-8}$  M to  $5 \times 10^{-6}$  M (Table 1).

**Table 1**

**Dissociation constants of Nanobodies against metal binding domains of ATP7B**

Nanobody	Target domain	$K_d$ (M) for Nanobody binding to MBD1-4 variants		
		<i>Apo</i> -MBD1-4	Cu-MBD1-4	SxxS-MBD1-4
<b>3ATP7</b>	MBD1	$4.3 \pm 1.9 \times 10^{-6}$	$2.6 \pm 0.6 \times 10^{-7}$	No binding
<b>3ATP145</b>		$1.9 \pm 1.8 \times 10^{-6}$	$3.2 \times 10^{-8}$	$2.1 \times 10^{-6}$
<b>3MBD10</b>	MBD2	$3.9 \pm 1.1 \times 10^{-7}$	$3.4 \pm 3.1 \times 10^{-7}$	$4.9 \pm 6.3 \times 10^{-6}$
<b>3MBD24</b>		$4.9 \pm 4.1 \times 10^{-6}$	$1.8 \pm 1.0 \times 10^{-7}$	$1.1 \pm 0.6 \times 10^{-7}$
<b>2R50</b>	MBD3	$5.0 \pm 1.7 \times 10^{-7}$	$1.4 \pm 1.3 \times 10^{-7}$	$1.4 \pm 0.1 \times 10^{-7}$
<b>1R1</b>	MBD4	$3.6 \pm 2.1 \times 10^{-8}$	n.d. <sup>1</sup>	n.d.
<b>4A19</b>		$1.3 \pm 0.2 \times 10^{-7}$	n.d.	$1.3 \pm 0.1 \times 10^{-6}$
<b>2R21<sup>2</sup></b>		$3.7 \pm 1.6 \times 10^{-8}$	$<1.0 \times 10^{-9}$	$4.9 \pm 2.1 \times 10^{-8}$

<sup>1</sup>n.d. –not determined

<sup>2</sup>  $K_d$  values less than  $10^{-9}$  M cannot be accurately measured by ITC directly.

Generally, Nanobodies targeting MBD3 or MBD4 had higher binding affinity than Nanobodies against MBD1 and MBD2. This appears to be reflected in the Nanobody reactivity on the Western blots. While all the tested Nanobodies reacted with the purified MBD1-4 and MBD1-6 (5  $\mu$ g per

band), only the Nanobodies against MBD3 and MBD4 were sensitive enough to detect the full-length ATP7B in the membrane preparations, where ATP7B was not detectable by Coomassie staining (less than 0.1  $\mu\text{g}$  per band, Figs. S1, S3). Interestingly, binding mechanism appeared to be different for these two Nanobody groups as well. While free energy change ( $\Delta G$ ) for Nanobody binding to MBD3 and, in particular, to MBD4 had strong enthalpic contribution, Nanobody binding to MBD1 and MBD2 was mostly entropy driven (Fig. 3, Fig. S4). This is significant, because, based on the NMR relaxation behavior of MBD1-6, we have previously proposed that MBD1-3 form a dynamically associated group maintained by relatively weak domain-domain interactions. Nanobody binding to MBD1 or MBD2 may disrupt these interactions, increasing the domain freedom of motion, and, consequently, entropy of the system.

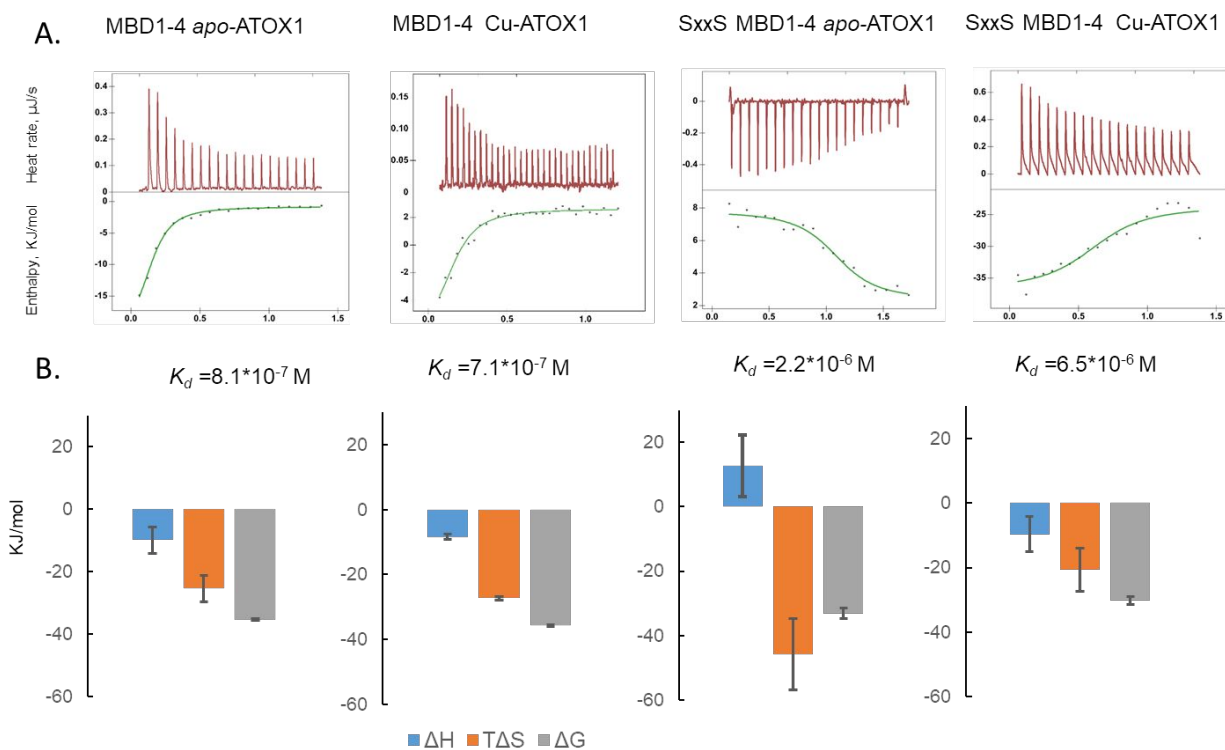


**Fig. 4 Thermodynamic parameters of Atox1 binding to MBD1-4. (A)** Thermograms and dissociation constants of Atox1 binding to MBD1-4. **(B)** Enthalpic and entropic contributions to the free energy change of Atox1 binding.

Several Nanobodies, including 2R21 (MBD4), 3MBD24 (MBD2) and 3ATP7 (MBD1) showed significantly stronger binding to the copper-loaded, than to the metal-free MBD1-4 (Table. 1). The 2R21 Nanobody was among those raised against copper-loaded MBD1-6<sup>14</sup>, and therefore stronger binding to Cu-MBD1-4, than to the metal-free protein may be expected, if the copper-binding site contributes to the epitope. Stronger binding to Cu-MBD1-4 for Nanobodies against MBD1 and

MBD2 is also consistent with better access to the binding sites in the open conformation of MBD1-3, where these MBDs have greater mobility.

Nanobodies against MBD2 could be uniquely useful as mimics of the copper chaperone ATOX1, the natural interaction partner of the metal-binding domains in ATP7B. ATOX1 was previously shown to preferentially transfer copper to MBD2<sup>41</sup>, and we have shown by NMR that *apo*-ATOX1 preferentially interacts with MBD2 in the context of MBD1-6 domain chain<sup>43</sup>. In fact, binding affinity of ATOX1 to MBD1-4 ( $K_d = 8.1 \times 10^{-7}$  M) was rather similar to the affinity of Nanobody 3MBD10, which targets MBD2 ( $K_d = 3.9 \times 10^{-7}$  M). Similar to 3MBD10, the  $\Delta G$  of ATOX1 interaction with MBD1-4 is also dominated by the entropic contribution (Fig. 4). In summary, the binding parameters of 3MBD10 Nanobody and ATOX1 are quite similar, and therefore using this Nanobody may allow separating the dynamic and conformational effects of ATOX1 binding to MBD1-6 domain chain from the copper transfer.

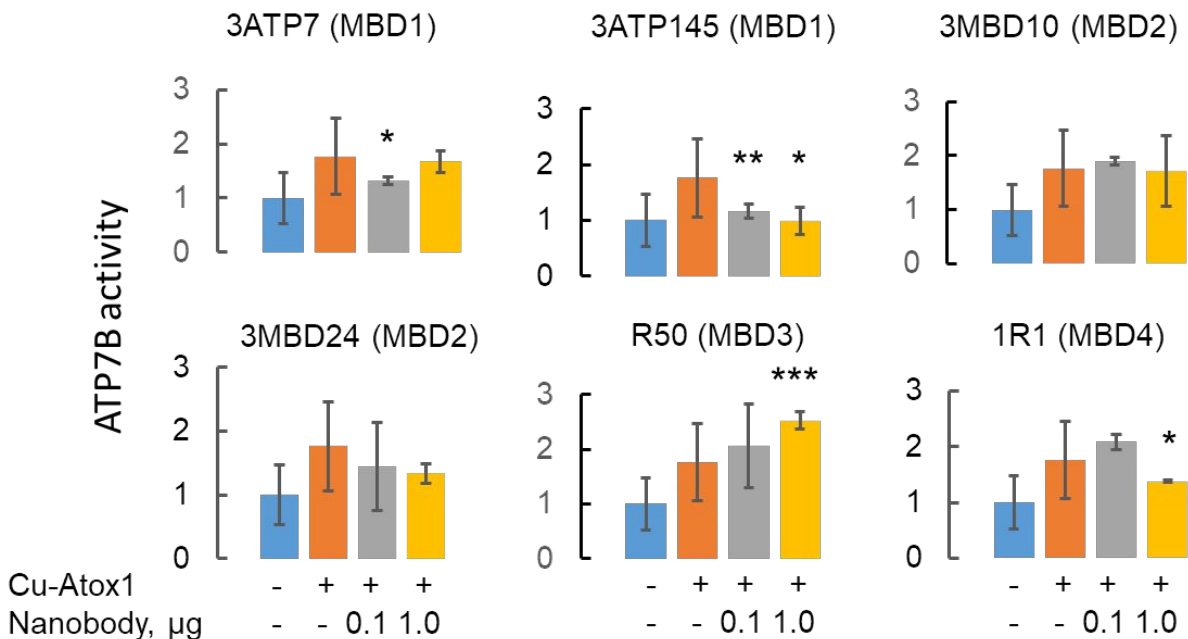


**Fig. 5 Effect of the Nanobodies on the ATPase activity of ATP7B in the membrane.** The activities were normalized to the specific activity of ATP7B without additions, which was  $3.5 \pm 1.6$  nmol/min mg protein. Statistically significant difference from the activity without Nanobody, in the presence of Atox1-Cu, is marked by the asterisks (\*,  $P < 0.05$ ; \*\*,  $P < 0.01$ ; \*\*\*,  $P < 0.001$ )

We have also tested binding of some Nanobodies to the MBD1-4 variant, where all four copper-binding CxxC motifs were replaced with SxxS (SxxS-MBD1-4, Table 1), making it unable to bind copper. Five of the tested Nanobodies showed similar binding affinities to the metal free MBD1-4 and to SxxS-MBD1-4, as expected. Interestingly, the 3ATP7 Nanobody targeting MBD1 showed no binding to SxxS-MBD1-4 at all, while 3MBD10 (MBD2) and 4A19 (MBD4) bound with a

1  
2  
3 lower affinity, as evidenced by about tenfold higher  $K_d$  value. This result likely indicates that for  
4 these Nanobodies, the CxxC copper binding motif forms a part of the epitope.  
5  
6

7 Our previous work indicates that ATP7B activity is regulated through the dynamic interactions  
8 between the MBDs<sup>43</sup>. Nanobody binding to the MBDs could disrupt domain-domain interactions,  
9 interfering with the activity regulation. We selected Nanobodies against each of the first four  
10 MBDs and tested their effect on the ATPase activity of ATP7B in the membrane (Fig. 5).  
11  
12

13 The wild type ATP7B, and the catalytically inactive D1027A variant were expressed in the  
14 mammalian HEK293 cells, and the ATP7B activity was measured as a difference between the rates  
15 of inorganic phosphate liberation by ATP hydrolysis in the wild type and the mutant membrane  
16 preparations. ATP hydrolysis in the P-type ATPases is tightly coupled to the ion translocation, and  
17 therefore ATPase activity is normally strongly stimulated by the transported ion. In the cell, copper  
18 is delivered to ATP7B by ATOX1, and, consequently, the ATPase activity of ATP7B *in vitro* is  
19 stimulated by ATOX1-Cu.  
20  
21  
22  
23

24 In our experiments, baseline ATP7B activity was  $3.5 \pm 1.6$  nmol/min  $\times$  mg protein and was  
25 stimulated by ATOX1-Cu to  $6.2 \pm 2.4$  nmol/min  $\times$  mg protein. Because the ATPase activity  
26 unrelated to ATP7B is subtracted, using catalytically inactive ATP7B as a control, the source of  
27 ATPase activity in the absence of ATOX1-Cu is unclear, and may be related to futile cycling of  
28 tightly bound copper within ATP7B. However, it is the ATOX1-Cu dependent fraction of activity  
29 that reflects physiological regulation of the ATP7B transporter. Nanobody 3ATP145 (MBD1)  
30 inhibited the total ATPase activity by approximately 45%, which corresponds to a complete  
31 inhibition of the ATOX1-Cu stimulated activity. Nanobody 1R1 (MBD4) also showed some  
32 inhibitory effect, approximately 20% of the total, or 50% of the ATOX1-Cu dependent ATPase  
33 activity. Interestingly, the 2R50 Nanobody against MBD3, which disrupts MBD1-3 interactions  
34 as shown by NMR<sup>14</sup>, stimulated the total ATP7B activity by approximately 50%. Inhibition of  
35 ATPase activity by the Nanobodies may have diverse causes, including interference with copper  
36 transfer from ATOX1, restricted MBD movements that affect intramolecular copper transfer or  
37 enzyme activation by copper, or steric hindrance of the global conformational changes associated  
38 with E1 to E2 transition in the course of the catalytic cycle. Activation of ATP7B by the 2R50  
39 Nanobody, on the other hand, is most likely explained by the dissociation of MBD1-3 domain  
40 group, which has been proposed to trigger activation of ATP7B<sup>43</sup>  
41  
42  
43  
44  
45  
46  
47

48 Detailed characterization of our panel of Nanobodies against ATP7B, identified several  
49 Nanobodies with particularly useful properties for the functional and structural studies of the  
50 copper transport processes. The 2R21 Nanobody has the highest affinity overall, with a  
51 dissociation constant for Cu-loaded MBD1-4 below  $10^{-9}$  M. Based on the high binding affinity,  
52 2R21, along with 1R1 and the already tested 5A51 (Fig. S3) should be particularly useful for  
53 immuno-affinity purification of ATP7B from the human tissues, e.g. for analysis of metal content  
54  
55  
56  
57  
58  
59  
60

1  
2  
3 and posttranslational modifications *in vivo*. These Nanobodies can be also used to stabilize the  
4 conformation of the highly mobile chain of the six metal binding domains in ATP7B for high  
5 resolution structure determination. The wide range of Nanobody affinities covering more than  
6 three orders of magnitude in terms of the dissociation constant is useful for protein dynamics  
7 studies by NMR, where a protein probe with moderate or low binding affinity is often a more  
8 useful tool than a tightly binding one.  
9  
10

11  
12 The 2R21, 3MBD24, and 3ATP145 Nanobodies show good discrimination between the copper-  
13 bound and metal-free form of the MBD chain, with at least tenfold affinity difference between the  
14 two. The 3ATP145 and 2R50 Nanobodies have opposite effects on ATP7B activity: whereas  
15 3ATP145 is strongly inhibiting, the 2R50 is activating. These properties should be particularly  
16 useful for in-cell studies of copper transport. Several Nanobodies show high specificity for  
17 particular MBDs, and allow selective targeting of either the MBD4, which plays mostly structural  
18 role, or the MBD1-3 domain group, which is involved in ATP7B regulation through domain  
19 dynamics.  
20  
21  
22  
23

24 Metal binding domains of ATP7B share high amino acid sequence similarity with the  
25 corresponding domains of the related human copper transporter ATP7A (between 40 and 60%  
26 identity for MBDs 1-4), and all the MBDs in ATP7B and ATP7A have very similar structure.  
27 Therefore, some Nanobodies may show cross-reactivity with ATP7A, especially if the epitope  
28 region includes the highly conserved sequence around the copper-binding CxxC motif. However,  
29 many epitopes are likely to be unique, because most Nanobodies do not show strong cross-  
30 reactivity with the other MBDs of ATP7B, even though amino acid identity between them can also  
31 reach 50%.  
32  
33  
34  
35

## 36 **Conclusions**

37  
38  
39 We have developed and characterized an arsenal of Nanobodies against human copper  
40 transporter ATP7B, with diverse properties, wide range of affinity and different domain specificity  
41 for studying the mechanism of ATP-driven copper transport *in vitro* and copper transport pathways  
42 in the cell. Several high-affinity Nanobodies targeting metal-binding domains 3 and 4 will likely  
43 be particularly useful for solving the high-resolution structure of ATP7B. Nanobodies against  
44 meta-binding domain 2 display similar binding properties to copper chaperone ATOX1,  
45 facilitating their use as ATOX1 mimics in dissecting the mechanism of intramolecular copper  
46 transfer in ATP7B. The activating and inhibitory Nanobodies can be used to manipulate ATP7B  
47 activity in the cell.  
48  
49  
50  
51  
52

## 53 **Conflicts of interest**

54  
55  
56  
57  
58  
59  
60

1  
2  
3 There are no conflicts to declare.  
4  
5

## 6 **Acknowledgments**

7

8 We are grateful to Dr. Marco Tonelli for collecting the NMR data, Dr. Scot Leary for his help in  
9 constructing GFP-ATP7B/mch46 cell line, to Dr. Samuel Jayakanthan for preparing the  
10 ATP7B/HEK293 membranes, and to Dr. Michal Boniecki for using instrumentation at the Protein  
11 Characterization and Crystallization Facility at the University of Saskatchewan.  
12  
13  
14

## 15 **Funding Information**

16

17 This work was supported by the NSERC Discovery grant to OD and by the National Institute of  
18 Health grant GM067166 to SL. NMR data were collected at the National Magnetic Resonance at  
19 Madison (NMRFAM), which is supported by NIH grant P41 GM103399 and by the University of  
20 Wisconsin-Madison. We thank SIBYLS beamline personnel at the Advanced Life Source for  
21 collecting SAXS data. ALS is supported by DOE Office of Biological and Environmental  
22 Research, NIH project ALS-ENABLE (P30 GM124169), and a High-End Instrumentation Grant  
23 S10OD018483.  
24  
25  
26  
27

## 28 **References**

29  
30  
31

- 32 1. Hamers-Casterman, C., Atarhouch, T., Muyldermans, S., Robinson, G., Hamers, C.,  
33 Songa, E. B., Bendahman, N., and Hamers, R. (1993) Naturally occurring antibodies  
34 devoid of light chains *Nature* 363, 446-448  
35
- 36 2. Pardon, E., Laeremans, T., Triest, S., Rasmussen, S. G., Wohlkonig, A., Ruf, A.,  
37 Muyldermans, S., Hol, W. G., Kobilka, B. K., and Steyaert, J. (2014) A general protocol  
38 for the generation of Nanobodies for structural biology *Nat. Protoc.* 9, 674-693  
39
- 40 3. Baranova, E., Fronzes, R., Garcia-Pino, A., Van, G. N., Papapostolou, D., Pehau-Arnaudet,  
41 G., Pardon, E., Steyaert, J., Howorka, S., and Remaut, H. (2012) SbsB structure and lattice  
42 reconstruction unveil Ca<sup>2+</sup> triggered S-layer assembly *Nature* 487, 119-122  
43
- 44 4. Ehrnstorfer, I. A., Geertsma, E. R., Pardon, E., Steyaert, J., and Dutzler, R. (2014) Crystal  
45 structure of a SLC11 (NRAMP) transporter reveals the basis for transition-metal ion  
46 transport *Nat. Struct. Mol. Biol.* 21, 990-996  
47
- 48 5. Hassaine, G., Deluz, C., Grasso, L., Wyss, R., Tol, M. B., Hovius, R., Graff, A., Stahlberg,  
49 H., Tomizaki, T., Desmyter, A., Moreau, C., Li, X. D., Poitevin, F., Vogel, H., and Nury,  
50 H. (2014) X-ray structure of the mouse serotonin 5-HT<sub>3</sub> receptor *Nature* 512, 276-281  
51  
52  
53  
54  
55  
56  
57  
58  
59  
60

- 1  
2  
3 6. Korotkov, K. V., Pardon, E., Steyaert, J., and Hol, W. G. (2009) Crystal structure of the N-  
4 terminal domain of the secretin GspD from ETEC determined with the assistance of a  
5 nanobody *Structure*. 17, 255-265  
6
- 7  
8 7. Pathare, G. R., Nagy, I., Sledz, P., Anderson, D. J., Zhou, H. J., Pardon, E., Steyaert, J.,  
9 Forster, F., Bracher, A., and Baumeister, W. (2014) Crystal structure of the proteasomal  
10 deubiquitylation module Rpn8-Rpn11 *Proc. Natl. Acad. Sci. U. S. A* 111, 2984-2989  
11
- 12 8. Rasmussen, S. G., Choi, H. J., Fung, J. J., Pardon, E., Casarosa, P., Chae, P. S., DeVree,  
13 B. T., Rosenbaum, D. M., Thian, F. S., Kobilka, T. S., Schnapp, A., Konetzki, I., Sunahara,  
14 R. K., Gellman, S. H., Pautsch, A., Steyaert, J., Weis, W. I., and Kobilka, B. K. (2011)  
15 Structure of a nanobody-stabilized active state of the beta(2) adrenoceptor *Nature* 469,  
16 175-180  
17
- 18  
19 9. Ring, A. M., Manglik, A., Kruse, A. C., Enos, M. D., Weis, W. I., Garcia, K. C., and  
20 Kobilka, B. K. (2013) Adrenaline-activated structure of beta2-adrenoceptor stabilized by  
21 an engineered nanobody *Nature* 502, 575-579  
22
- 23 10. Uchanski, T., Pardon, E., and Steyaert, J. (2020) Nanobodies to study protein  
24 conformational states *Curr. Opin. Struct. Biol.* 60, 117-123  
25
- 26 11. Ward, A. B., Szewczyk, P., Grimard, V., Lee, C. W., Martinez, L., Doshi, R., Caya, A.,  
27 Villaluz, M., Pardon, E., Cregger, C., Swartz, D. J., Falson, P. G., Urbatsch, I. L., Govaerts,  
28 C., Steyaert, J., and Chang, G. (2013) Structures of P-glycoprotein reveal its  
29 conformational flexibility and an epitope on the nucleotide-binding domain *Proc. Natl.*  
30 *Acad. Sci. U. S. A* 110, 13386-13391  
31  
32
- 33 12. De Genst E., Chan, P. H., Pardon, E., Hsu, S. T., Kumita, J. R., Christodoulou, J., Menzer,  
34 L., Chirgadze, D. Y., Robinson, C. V., Muyldermans, S., Matagne, A., Wyns, L., Dobson,  
35 C. M., and Dumoulin, M. (2013) A nanobody binding to non-amyloidogenic regions of the  
36 protein human lysozyme enhances partial unfolding but inhibits amyloid fibril formation  
37 *J. Phys. Chem. B* 117, 13245-13258  
38  
39
- 40 13. Dmitriev, O. Y., Lutsenko, S., and Muyldermans, S. (2016) Nanobodies as Probes for  
41 Protein Dynamics in Vitro and in Cells *J. Biol. Chem.* 291, 3767-3775  
42
- 43 14. Huang, Y., Nokhrin, S., Hassanzadeh-Ghassabeh, G., Yu, C. H., Yang, H., Barry, A. N.,  
44 Tonelli, M., Markley, J. L., Muyldermans, S., Dmitriev, O. Y., and Lutsenko, S. (2014)  
45 Interactions between metal-binding domains modulate intracellular targeting of Cu(I)-  
46 ATPase ATP7B, as revealed by nanobody binding *J. Biol. Chem.* 289, 32682-32693  
47  
48
- 49 15. Gerdes, C., Waal, N., Offner, T., Fornasiero, E. F., Wender, N., Verbar, H., Manzini, I.,  
50 Trenkwalder, C., Mollenhauer, B., Strohaber, T., Zweckstetter, M., Becker, S., Rizzoli, S.  
51 O., Basmanav, F. B., and Opazo, F. (2020) A nanobody-based fluorescent reporter reveals  
52 human alpha-synuclein in the cell cytosol *Nat. Commun.* 11, 2729  
53  
54  
55  
56  
57  
58  
59  
60

16. Ghosh, R. P., Franklin, J. M., Draper, W. E., Shi, Q., Beltran, B., Spakowitz, A. J., and Liphardt, J. T. (2019) A fluorogenic array for temporally unlimited single-molecule tracking *Nat. Chem. Biol.* 15, 401-409
17. Derivery, E., Seum, C., Daeden, A., Loubery, S., Holtzer, L., Julicher, F., and Gonzalez-Gaitan, M. (2015) Polarized endosome dynamics by spindle asymmetry during asymmetric cell division *Nature* 528, 280-285
18. Heinz, K. S. and Cardoso, M. C. (2019) Targeted Manipulation/Repositioning of Subcellular Structures and Molecules *Methods Mol. Biol.* 2038, 199-208
19. Steels, A., Verhelle, A., Zwaenepoel, O., and Gettemans, J. (2018) Intracellular displacement of p53 using transactivation domain (p53 TAD) specific nanobodies *MAbs.* 10, 1045-1059
20. Daniel, K., Icha, J., Horenburg, C., Muller, D., Norden, C., and Mansfeld, J. (2018) Conditional control of fluorescent protein degradation by an auxin-dependent nanobody *Nat. Commun.* 9, 3297
21. Kanner, S. A., Morgenstern, T., and Colecraft, H. M. (2017) Sculpting ion channel functional expression with engineered ubiquitin ligases *Elife.* 6,
22. Yamaguchi, N., Colak-Champollion, T., and Knaut, H. (2019) zGrad is a nanobody-based degron system that inactivates proteins in zebrafish *Elife.* 8,
23. Bruce, V. J., Lopez-Islas, M., and McNaughton, B. R. (2016) Resurfaced cell-penetrating nanobodies: A potentially general scaffold for intracellularly targeted protein discovery *Protein Sci.* 25, 1129-1137
24. Herce, H. D., Schumacher, D., Schneider, A. F. L., Ludwig, A. K., Mann, F. A., Fillies, M., Kasper, M. A., Reinke, S., Krause, E., Leonhardt, H., Cardoso, M. C., and Hackenberger, C. P. R. (2017) Cell-permeable nanobodies for targeted immunolabelling and antigen manipulation in living cells *Nat. Chem.* 9, 762-771
25. Jovcevska, I. and Muyldermans, S. (2020) The Therapeutic Potential of Nanobodies *BioDrugs.* 34, 11-26
26. Lecocq, Q., De, V. Y., Hanssens, H., D'Huyvetter, M., Raes, G., Goyvaerts, C., Keyaerts, M., Devoogdt, N., and Breckpot, K. (2019) Theranostics in immuno-oncology using nanobody derivatives *Theranostics.* 9, 7772-7791
27. Messer, A. and Butler, D. C. (2020) Optimizing intracellular antibodies (intrabodies/nanobodies) to treat neurodegenerative disorders *Neurobiol. Dis.* 134, 104619
28. Wrapp, D., De, V. D., Corbett, K. S., Torres, G. M., Wang, N., Van, B. W., Roose, K., van, S. L., Hoffmann, M., Pohlmann, S., Graham, B. S., Callewaert, N., Schepens, B., Saelens, X., and McLellan, J. S. (2020) Structural Basis for Potent Neutralization of Betacoronaviruses by Single-Domain Camelid Antibodies *Cell* 181, 1004-1015

- 1
  - 2
  - 3
  - 4
  - 5
  - 6
  - 7
  - 8
  - 9
  - 10
  - 11
  - 12
  - 13
  - 14
  - 15
  - 16
  - 17
  - 18
  - 19
  - 20
  - 21
  - 22
  - 23
  - 24
  - 25
  - 26
  - 27
  - 28
  - 29
  - 30
  - 31
  - 32
  - 33
  - 34
  - 35
  - 36
  - 37
  - 38
  - 39
  - 40
  - 41
  - 42
  - 43
  - 44
  - 45
  - 46
  - 47
  - 48
  - 49
  - 50
  - 51
  - 52
  - 53
  - 54
  - 55
  - 56
  - 57
  - 58
  - 59
  - 60
29. Scully, M., Cataland, S. R., Peyvandi, F., Coppo, P., Knobl, P., Kremer Hovinga, J. A., Metjian, A., de la Rubia, J., Pavenski, K., Callewaert, F., Biswas, D., De, W. H., and Zeldin, R. K. (2019) Caplacizumab Treatment for Acquired Thrombotic Thrombocytopenic Purpura *N. Engl. J. Med.* 380, 335-346
30. Hasan, N. M. and Lutsenko, S. (2012) Regulation of copper transporters in human cells *Curr. Top. Membr.* 69, 137-161
31. Danks, D. M. (1995) Disorders of Copper Transport. In Scriver, C. R., editor. *The Metabolic and Molecular Bases of Inherited Disease*, McGraw-Hill, Inc., New York
32. Schilsky, M. L. (2017) Wilson Disease: Diagnosis, Treatment, and Follow-up *Clin. Liver Dis.* 21, 755-767
33. Toyoshima, C., Nakasako, M., Nomura, H., and Ogawa, H. (2000) Crystal structure of the calcium pump of sarcoplasmic reticulum at 2.6 Å resolution *Nature* 405, 647-655
34. Morth, J. P., Pedersen, B. P., Toustrup-Jensen, M. S., Sorensen, T. L., Petersen, J., Andersen, J. P., Vilsen, B., and Nissen, P. (2007) Crystal structure of the sodium-potassium pump *Nature* 450, 1043-1049
35. Wernimont, A. K., Huffman, D. L., Lamb, A. L., O'Halloran, T. V., and Rosenzweig, A. C. (2000) Structural basis for copper transfer by the metallochaperone for the Menkes/Wilson disease proteins *Nat. Struct. Biol.* 7, 766-771
36. Banci, L., Bertini, I., Cantini, F., Massagni, C., Migliardi, M., and Rosato, A. (2009) An NMR study of the interaction of the N-terminal cytoplasmic tail of the Wilson disease protein with copper(I)-HAH1 *J. Biol. Chem.* 284, 9354-9360
37. Fatemi, N., Korzhnev, D. M., Velyvis, A., Sarkar, B., and Forman-Kay, J. D. (2010) NMR characterization of copper-binding domains 4-6 of ATP7B *Biochemistry* 49, 8468-8477
38. Achila, D., Banci, L., Bertini, I., Bunce, J., Ciofi-Baffoni, S., and Huffman, D. L. (2006) Structure of human Wilson protein domains 5 and 6 and their interplay with domain 4 and the copper chaperone HAH1 in copper uptake *Proc. Natl. Acad. Sci. U. S. A* 103, 5729-5734
39. Bartee, M. Y., Ralle, M., and Lutsenko, S. (2009) The loop connecting metal-binding domains 3 and 4 of ATP7B is a target of a kinase-mediated phosphorylation *Biochemistry* 48, 5573-5581
40. LeShane, E. S., Shinde, U., Walker, J. M., Barry, A. N., Blackburn, N. J., Ralle, M., and Lutsenko, S. (2010) Interactions between Copper-binding Sites Determine the Redox Status and Conformation of the Regulatory N-terminal Domain of ATP7B *J. Biol. Chem.* 285, 6327-6336

- 1
- 2
- 3
- 4 41. Walker, J. M., Huster, D., Ralle, M., Morgan, C. T., Blackburn, N. J., and Lutsenko, S. (2004) The N-terminal metal-binding site 2 of the Wilson's Disease Protein plays a key
- 5 role in the transfer of copper from Atox1 *J. Biol. Chem.* 279, 15376-15384
- 6
- 7
- 8 42. Yatsunyk, L. A. and Rosenzweig, A. C. (2007) Cu(I) binding and transfer by the N
- 9 terminus of the Wilson disease protein *J. Biol. Chem.* 282, 8622-8631
- 10
- 11 43. Yu, C. H., Yang, N., Bothe, J., Tonelli, M., Nokhrin, S., Dolgova, N. V., Braiterman, L.,
- 12 Lutsenko, S., and Dmitriev, O. Y. (2017) The metal chaperone Atox1 regulates the activity
- 13 of the human copper transporter ATP7B by modulating domain dynamics *J. Biol. Chem.*
- 14 292, 18169-18177
- 15
- 16 44. Jayakanthan, S., Braiterman, L. T., Hasan, N. M., Unger, V. M., and Lutsenko, S. (2017)
- 17 Human copper transporter ATP7B (Wilson disease protein) forms stable dimers in vitro
- 18 and in cells *J. Biol. Chem.* 292, 18760-18774
- 19
- 20
- 21 45. Lanzetta, P. A., Alvarez, L. J., Reinach, P. S., and Candia, O. A. (1979) An improved assay
- 22 for nanomole amounts of inorganic phosphate *Anal. Biochem.* 100, 95-97
- 23
- 24 46. Singh, K. and Shukla, A. K. (2003) Poly-vinyl alcohol (PVA) and malachite green: a new
- 25 reagent system for the microdetermination of phosphate in water and wastewater *Indian J.*
- 26 *Environ. Health* 45, 203-208
- 27
- 28
- 29 47. Putnam, C. D., Hammel, M., Hura, G. L., and Tainer, J. A. (2007) X-ray solution scattering
- 30 (SAXS) combined with crystallography and computation: defining accurate
- 31 macromolecular structures, conformations and assemblies in solution *Q. Rev. Biophys.* 40,
- 32 191-285
- 33
- 34 48. Franke, D. and Svergun, D. I. (2009) DAMMIF, a program for rapid ab-initio shape
- 35 determination in small-angle scattering *J. Appl. Crystallogr.* 42, 342-346
- 36
- 37
- 38 49. Volkov, V. and Svergun, D. I. (2003) Uniqueness of ab-initio shape determination in small-
- 39 angle scattering *J. Appl. Crystallogr.* 36,
- 40
- 41 50. van Zundert, G. C. P., Rodrigues, J. P. G. L., Trellet, M., Schmitz, C., Kastiris, P. L.,
- 42 Karaca, E., Melquiond, A. S. J., van, D. M., de Vries, S. J., and Bonvin, A. M. J. J. (2016)
- 43 The HADDOCK2.2 Web Server: User-Friendly Integrative Modeling of Biomolecular
- 44 Complexes *J. Mol. Biol.* 428, 720-725
- 45
- 46 51. Petoukhov, M. V. and Svergun, D. I. (2005) Global rigid body modeling of
- 47 macromolecular complexes against small-angle scattering data *Biophys. J.* 89, 1237-1250
- 48
- 49
- 50 52. Pervushin, K., Riek, R., Wider, G., and Wuthrich, K. (1997) Attenuated T2 relaxation by
- 51 mutual cancellation of dipole-dipole coupling and chemical shift anisotropy indicates an
- 52 avenue to NMR structures of very large biological macromolecules in solution *Proc. Natl.*
- 53 *Acad. Sci. U. S. A* 94, 12366-12371
- 54
- 55
- 56
- 57
- 58
- 59
- 60

- 1  
2  
3 53. Schagger, H. and von Jagow, G. (1987) Tricine-sodium dodecyl sulfate-polyacrylamide  
4 gel electrophoresis for the separation of proteins in the range from 1 to 100 kDa *Anal.*  
5 *Biochem.* 166, 368-379  
6  
7 54. Laemmli, U. K. (1970) Cleavage of structural proteins during the assembly of the head of  
8 bacteriophage T4 *Nature* 227, 680-685  
9  
10  
11  
12  
13  
14  
15  
16  
17  
18  
19  
20  
21  
22  
23  
24  
25  
26  
27  
28  
29  
30  
31  
32  
33  
34  
35  
36  
37  
38  
39  
40  
41  
42  
43  
44  
45  
46  
47  
48  
49  
50  
51  
52  
53  
54  
55  
56  
57  
58  
59  
60